Supporting Information

S1 Crystal structure of cubic and tetragonal $BaTiO_3$ nanocubes

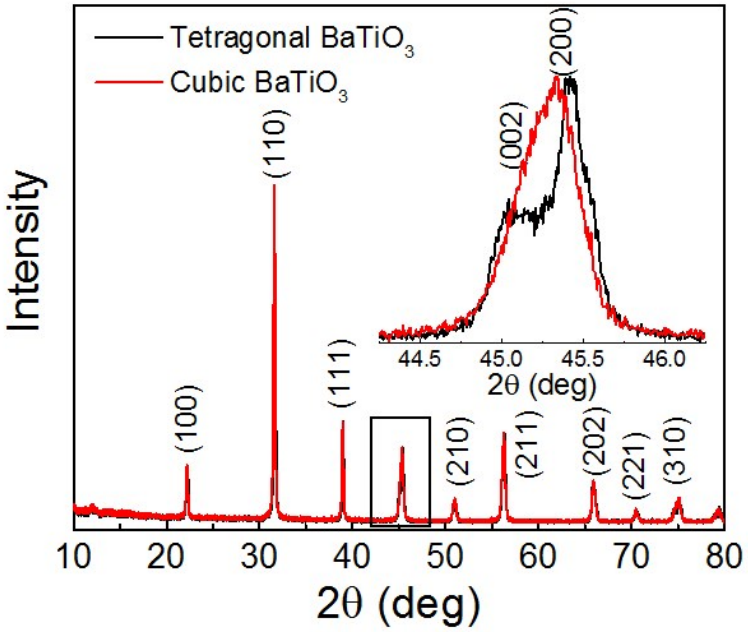

Fig. S1 XRD pattern of tetragonal and cubic $BaTiO_3$ nanocubes. Enlargement of (002, 200) peaks (insert) in the 2θ range of 44°-46°.

The phase composition of the powders prepared by the two synthesis methods was investigated by XRD. The diffraction peaks can be easily identified for the two kinds of $BaTiO_3$ (Fig. S1). Black curve in Fig. S1 shows the XRD pattern of the nanocubes synthesized by a composite hydroxide-mediated method. Which can be indexed as tetragonal $BaTiO_3$ with space group P4mm (PDF card no. 75-1606). The peak splitting of (002) and (200) at 2θ～45° confirms that the nanoparticle is tetragonal ferroelectric $BaTiO_3$ (insert in Fig. S1). The calculated lattice parameters corresponding from the XRD data are: a=0.399 nm and c=0.403 nm. However, similar peak splitting is not observed in the XRD patterns of as-synthesized sample through hydrothermal method (red curve). Thus, these crystallites have a cubic structure. The schematic crystal structure of cubic and tetragonal $BaTiO_3$ nanocubes were shown in Fig S2.

For cubic $BaTiO_3$, the structure of which is displayed in Fig. S2a, titanium atoms are octahedrally coordinated by six oxygen atoms. Ferroelectricity in tetragonal $BaTiO_3$ is due to an average relative displacement along the c-axis of titanium from its centrosymmetric position in the unit cell and consequently the creation of a permanent electric dipole. The tetragonal unit cell is shown in Fig. S2b. The elongation of the unit cell along the c-axis and consequently the deviation of the c/a ratio from unity are used as an indication of the presence of the ferroelectric phase.

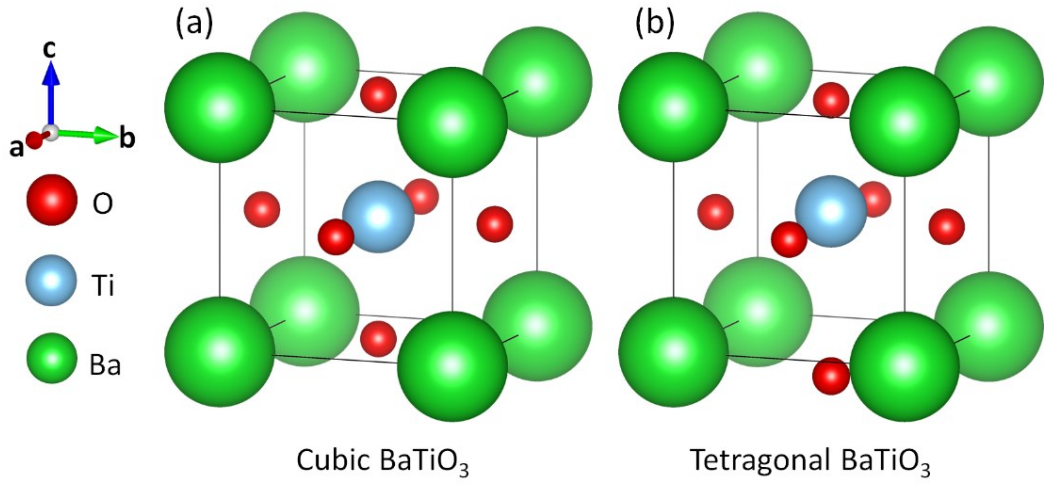

Fig S2 Schematic crystal structure of cubic and tetragonal $BaTiO_3$ nanocubes Unit cell of $BaTiO_3$ in both the (a) cubic Pm-3m structure and (b) tetragonal P4mm structure. In the tetragonal unit cell, atoms are displaced in the z-direction, and the cell is elongated along the c axis. Atom positions: Ba at (0, 0, 0); Ti at (1/2, 1/2, z); O1 at (1/2, 1/2, z); and O2 at (1/2, 0, z). Displacements have been exaggerated for clarity.

S2 Morphology of cubic and tetragonal $BaTiO_3$ nanocubes

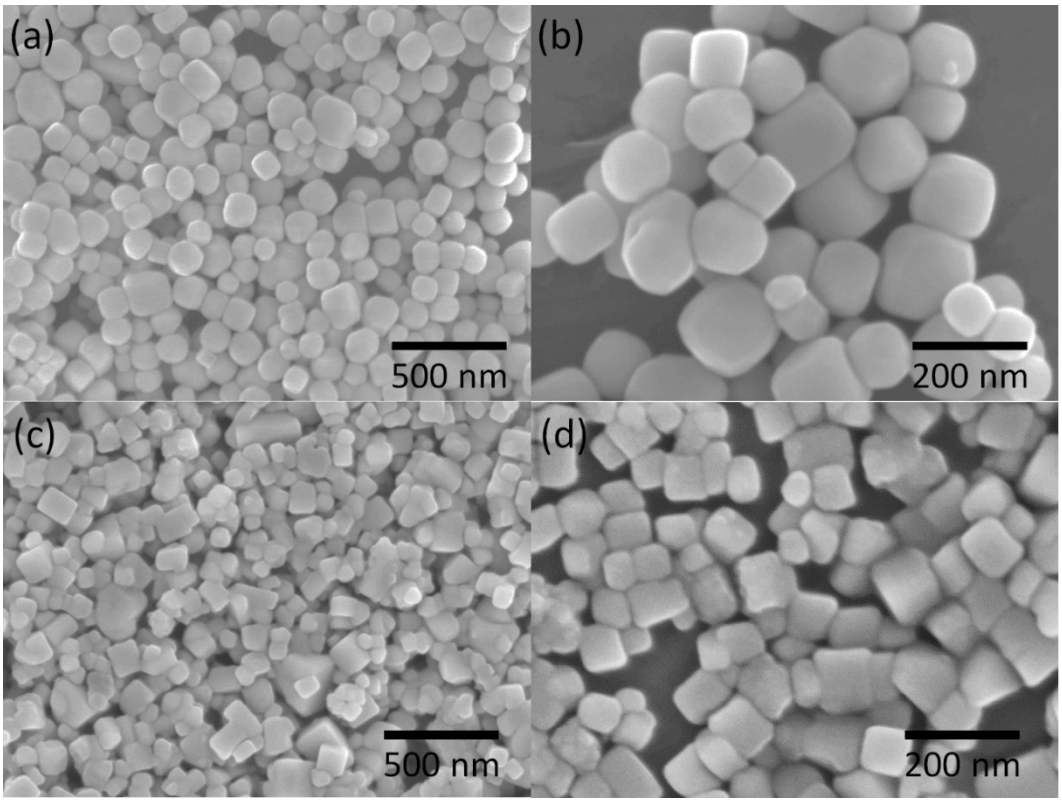

Fig. S3 SEM images of cubic (a,b) and tetragonal (c,d) $BaTiO_3$ nanocubes

The morphology of the two types of powders were investigated by SEM. And the SEM images of the cubic $BaTiO_3$ power is shown in Fig. S3a and 3b. Most of the particles prepared by hydrothermal method have an arc-shaped chamfered cubic shape with near-spherical shape. For the tetragonal $BaTiO_3$ power synthesized through the composite-hydroxide-mediated (CHM) approach, most of the nanoparticles also have a cube-like morphology, but a few of them are cuboids with relatively flat facets (Fig. S3c and 3d). The statistical average size of the two types of $BaTiO_3$ nanocubes obtained by measuring and averaging 100 particles from the SEM images is 86.99 and 87.72nm, respectively (Fig. S4).

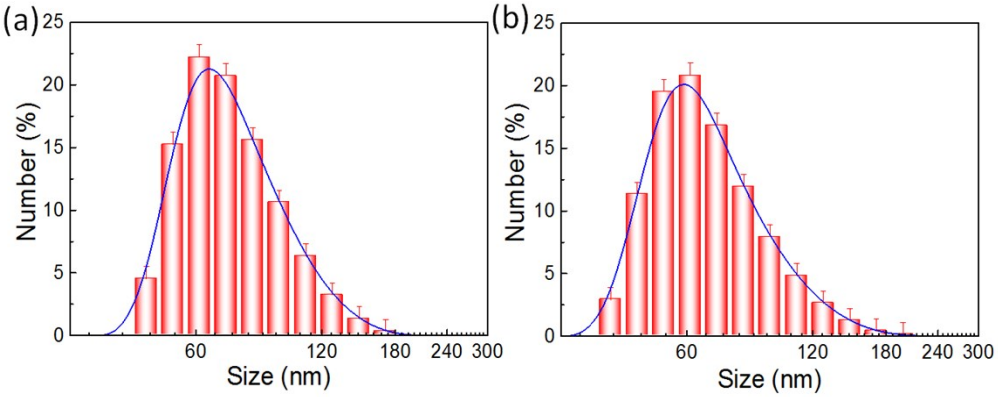

Fig. S4 Particle size distribution of cubic (a) and tetragonal (b) $BaTiO_3$ nanocubes

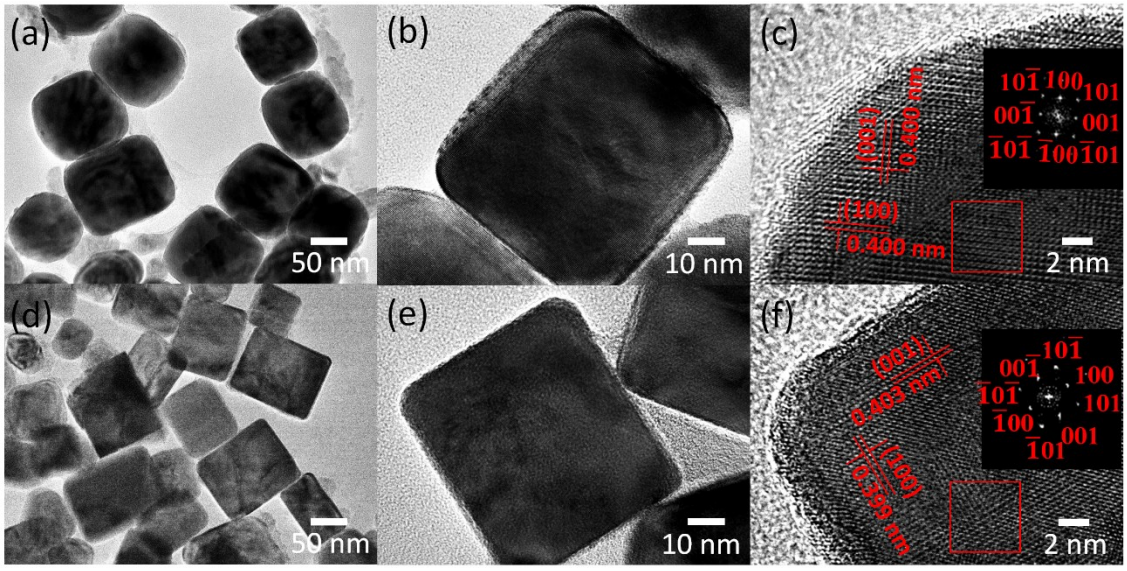

Fig. S5 TEM images of cubic (a,b) and tetragonal (d,e) $BaTiO_3$ nanocubes at different magnifications; HRTEM images and fast Fourier transform pattern (insert) of cubic (c) and tetragonal (f) $BaTiO_3$

TEM images with different magnifications of two samples (Fig. S5) further demonstrate the size and cube-like morphology of the two $BaTiO_3$ nanoparticles and are consistent with

the SEM results. Compared to cubic $BaTiO_3$ nanocubes, the surfaces of tetragonal BaTiO3 nanocubes are flatter with regular rectangular. The HRTEM image of the two types of $BaTiO_3$ nanocubes and the fast Fourier transform pattern of an individual $BaTiO_3$ nanocube show that they are all defect-free single nanocrystal grown along the (100) plane (Fig. S5c, 5f and inserts). From Fig. S5c, it can be seen that the measured interplanar distances are ca. 0.400 and 0.400 nm, which are consistent with the results from XRD, corresponding to the (001) and (100) planes of $BaTiO_3$, respectively, further confirming that the $BaTiO_3$ crystal possesses a cubic Pm-3m structure. However, from Fig S5f, planes with spacing of ca. 0.403 and 0.399 nm corresponding to the (001) and (100) planes of $BaTiO_3$ nanocubes, which are in agreement with the results from XRD, and it is further demonstrated that the $BaTiO_3$ crystal possesses a tetragonal P4mm structure.

S3 Photocatalytic H_2 evolution from an aqueous methanol solution

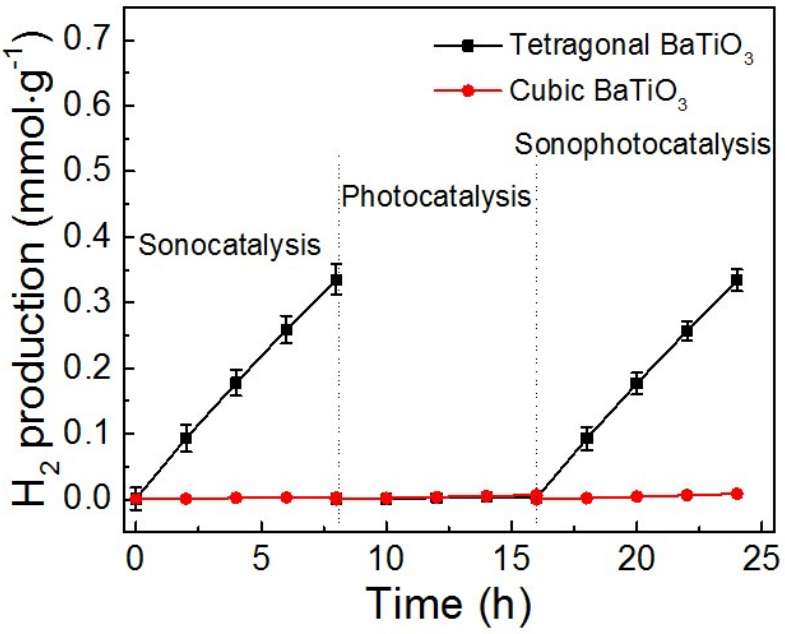

Fig S6 H_2 evolution performance as a function of irradiation time for sonocatalysis, photocatalysis and sonophotocatalysis in the presence of cubic and tetragonal $BaTiO_3$

As reported in the previous papers, Kuang-Sheng Hong et. al. proposed a mechanism of the piezoelectrochemical effect for the direct conversion of mechanical energy to chemical energy. Based on this mechanism, they did experiment to split water for generating hydrogen and oxygen by means of as-synthesized piezoelectric ZnO microfibers and $BaTiO_3$ microdendrites under ultrasonic irradiation. Dendrites are vibrated with ultrasonic waves, leading to a strain-induced electric charge development on their surface. With sufficient electric potential, strained piezoelectric dendrites in water triggered the redox reaction of water to produce hydrogen and oxygen gases.

To verify the mechanism we proposed, we evaluated the water splitting performance of $BaTiO_3$ nanocubes alone under ultrasonic irradiation only in methanol water solution (methanol:water=1:4). Fig. S6 shows the evolution of H_2 from as-synthesized $BaTiO_3$ nanocube (100mg), with an average rate of H_2 evolution of approximately 41.16 $\mu mol \cdot g^{-1} \cdot h^{-1}$ in the first vibration event (0-8h). Gas generation stops without ultrasonic irradiation (8-16 h, Fig. S6). This result indicates that the splitting reaction of the water can be induced by external mechanical energy without assist of other form of energy. As seen in Fig. S6, when the ultrasonic irradiation is off, $BaTiO_3$ nanocubes stop to generate hydrogen and oxygen without acoustic pressure and cavitation induced by ultrasonic wave. After evacuating the reaction system and starting the ultrasonic irradiation again, a similar H_2 producing rate regained. As well known, the water-splitting effect is thought as powerful evidence of the release of free charge carriers into reaction system. Therefore, this result could demonstrate a strain-induced electric charge development on their surface. Thus, ultrasonic driven piezoelectric effect of ferroelectric $BaTiO_3$ nanocubes can induce the release of free charge carriers into reaction system. It is consistent with the electro-catalysis mechanism proposed by Kuang-Sheng Hong et. al.

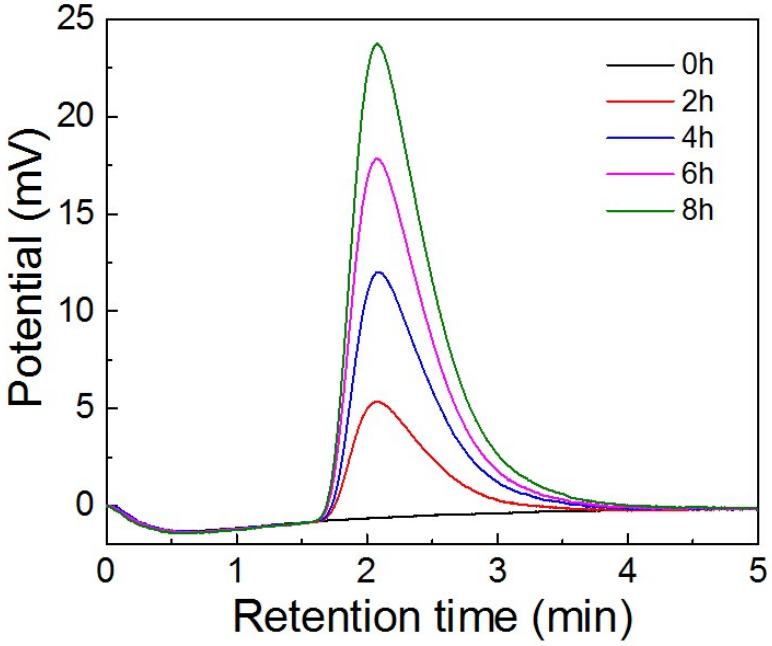

Fig S7 HPLC chromatography of H_2 as a function of irradiation time in presence of urchin-like $TiO_2/BaTiO_3$ hybrid microspheres with an effective mass of 100 mg in the system.

S4 SEM and TEM images of urchin-like $TiO_2/BaTiO_3$ hybrid microspheres after ultrasonic treatment

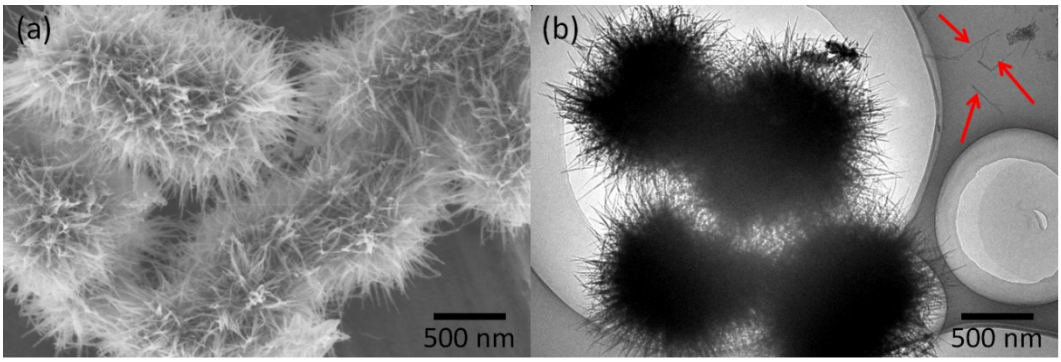

Fig S8 SEM and TEM image of urchin-like $TiO_2/BaTiO_3$ hybrid microspheres after ultrasonic treatment

To achieve good sonophotocatalytic performance for the urchin-like $TiO_2/BaTiO_3$ hybrid microspheres, the stability of this hybrid structure is crucial under ultrasonic treatment. The sample of hybrid nanocubes was dispersed in deionized water under ultrasonic treatment at 40 kHz, 50 W for 2h. Fig. S8 shows SEM and TEM images of the urchin-like $TiO_2/BaTiO_3$ hybrid microspheres after ultrasonic treatment. The TiO_2 nanowires are tightly attached on the surface of the $BaTiO_3$ nanocubes. There is few free TiO_2 nanowires in the suspension. This high stability of the hybrid structure enhances the electron transmission between the two phases under ultrasound irradiation.

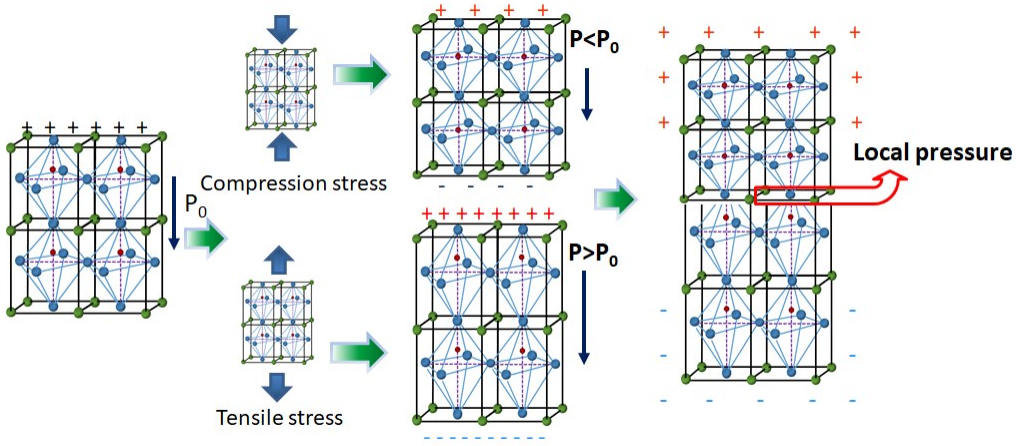

Fig S9 Effect of stress and local water pressure on polarization electric potential of $BaTiO_3$

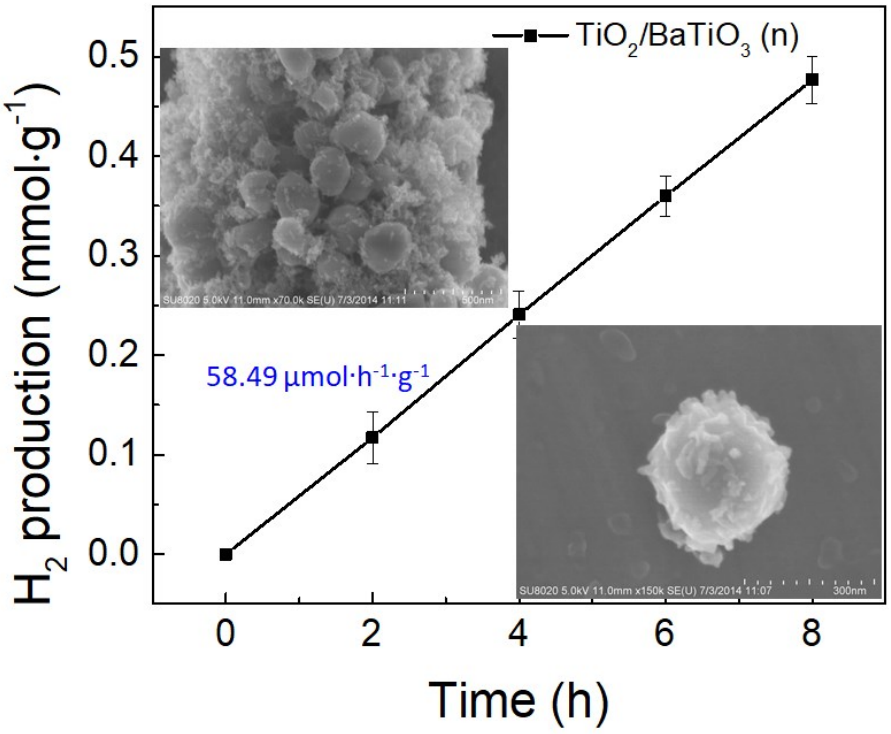

Fig S10 H_2 evolution performance as a function of irradiation time for sonophotocatalysis in the presence of $TiO_2/BaTiO_3$ hybrid microspheres (No CTAB in the synthesis process) and its corresponding SEM images insert.